Available online at www.sciencedirect.com

ScienceDirect

journal homepage: www.intl.elsevierhealth.com/journals/dema

Validation of in-vitro tests of zirconia-ceramic inlay-retained fixed partial dentures: A finite element analysis

M. Waldecker*,[1], S. Rues[1], P. Rammelsberg, W. Bömicke

Department of Prosthodontics, Heidelberg University Hospital, University of Heidelberg, Heidelberg, Germany

ARTICLE INFO

Article history:
Received 14 September 2018
Received in revised form
13 December 2018
Accepted 13 January 2019

Keywords:
Finite element analysis
Zirconia
All-ceramic
Inlay-retained fixed partial dentures
Fracture resistance

ABSTRACT

Objective. In the past, discrepancies between laboratory results and clinical behavior have been observed for all-ceramic restorations. This analysis of fracture resistance of zirconia-based inlay-retained fixed partial dentures (IRFPDs) aimed at identifying correlations between an in-vitro test setup and the clinical situation. The effects of tooth material, tooth mobility, restoration design, load direction, and different cements were taken into account.
Methods. The in-vitro test model and IRFPD were reverse engineered (Geomagic DesignX) and meshed predominantly with hexahedral elements (approx. 230,000 elements). Homogenous, linear-elastic behavior was assumed for all materials. On the basis of the calculated stresses (ANSYS 18.2) and already known strength distributions for the restorative materials fracture resistance of the complete restoration and force at initial damage (fracture within the veneer) was estimated on the basis of the principal stress hypothesis. Differences depending on the assumed clinical situation and effects of different variables on fracture resistance were evaluated.
Results. All variables tested in the finite element analysis affected the calculated fracture resistance of the IRFPD. Use of resin teeth led to an underestimation of fracture resistance by up to −57%, whereas fracture resistance of IRFPDs on metal abutment teeth was close to the clinical reference (−6% to +15%). Good correlation between the clinical scenario and that using metal teeth could only be achieved when the natural resilience of the abutment teeth was simulated.
Significance. When testing fracture resistance of zirconia-based IRFPDs, metal abutment teeth in combination with simulated tooth resilience can reflect the clinical situation accurately.

1. Introduction

Before clinical application of any new type of prosthetic restoration or material, its mechanical performance must be determined and evaluated in pre-clinical tests. If the fracture resistance of a restoration exceeds an expected maximum bite force, typically about 500 N in the molar region [1–3], it is not expected to suffer major damage in clinical use. The predictive power of pre-clinical tests depends to a large extent on

* *Corresponding author at*: Im Neuenheimer Feld 400, 69120, Heidelberg, Germany.
E-mail address: moritz.waldecker@med.uni-heidelberg.de (M. Waldecker).
[1] These authors contributed equally to this work.
https://doi.org/10.1016/j.dental.2019.01.017

the experimental setup, e.g. magnitude, frequency, and direction of the applied load or, more generally, on how well the clinical conditions are approximated. Extremely high fracture resistance and favorable fatigue behavior have been determined for fixed partial dentures (FPDs) made from zirconia compared with other dental ceramics, which is why zirconia FPDs have been recommended for the molar region [4,5]. It was subsequently clinically proved that zirconia frameworks could withstand the forces in the oral cavity in the long term [6]. It emerged, however, that the prognosis of zirconia-based restorations is restricted not by their frameworks, but by the fragility of their veneer [7]. In-vivo studies estimated the incidence of chipping for zirconia-based posterior FPDs to be 19–28% within the first three to seven years. [8–11]. The discrepancy between the fracture resistance determined in the laboratory and that determined for clinical performance was particularly large for inlay-retained FPDs (IRFPDs). Although the mean failure load of zirconia-based IRFPDs was >1000 N – >3000 N (assuming a minimum framework cross-section of 9 mm^2 in the connector area) [12–14] and fracture resistance of the veneer in the range 1276–1413 N was determined [15], they were highly susceptible to chipping and consequently low survival; this was ultimately also because of framework fractures [16]. This suggests that the high fracture resistance found in vitro may have been based on test protocols that were not rigorous enough to produce a clinically relevant damage pattern; these tests usually simulated axial load in which the force was applied centrally to the pontic. In addition, the tests focused almost exclusively on complete fractures; i.e., the occurrence of initial damage [17], for example in the veneer of the restorations [18,19], was not recorded, which may have contributed to an overestimation of the performance of the restorations. If, however, a more rigorous test setup was chosen (using an oblique load acting eccentrically on the pontic) and restorations were adequately observed during the fracture test, such initial damage was found to occur to both veneered conventional and inlay-retained FPDs at significantly lower loads than ultimate fracture loads, and below the clinically relevant threshold of 500 N, for approximately 25% of restorations [20,21]. To determine the fracture resistance of restorations under oblique loading conditions, all other components of the experimental setup must withstand the forces occurring during the fracture test. This means, for example, that metal abutments instead of natural teeth or resin abutments must be used. It has been shown, however, that abutment material can affect the fracture resistance of ceramic FPDs [22]. This also applies to other variables in the experimental setup, such as the resilience of the abutment teeth or the loading direction [23,24]. To further improve conclusions based on in-vitro test results, finite element analyses (FEAs) were conducted for an actual test setup [21] in which essential test variables were varied. FEA can be used to calculate the stress distribution within an FDP and subsequently estimate its load-bearing capacity [25]. Once a mathematical model has been established, many variables can be tested. In this way, FEA contributes to reducing the number of laboratory examinations and thus supports more cost-efficient development of dental prostheses. Cracking of a ceramic material usually occurs when the maximum first principle stress exceeds its tensile strength. Locations where critical tensile stresses occur first are often referred to as "weak points". In this study, FEA has been conducted to assess how the variables 'abutment material', 'resilience of the abutment', 'direction of the applied load', and 'stiffness of the cement layer' affect the fracture resistance of zirconia IRFPDs in an in-vitro test setup, and to correlate the findings with an assumed clinical situation.

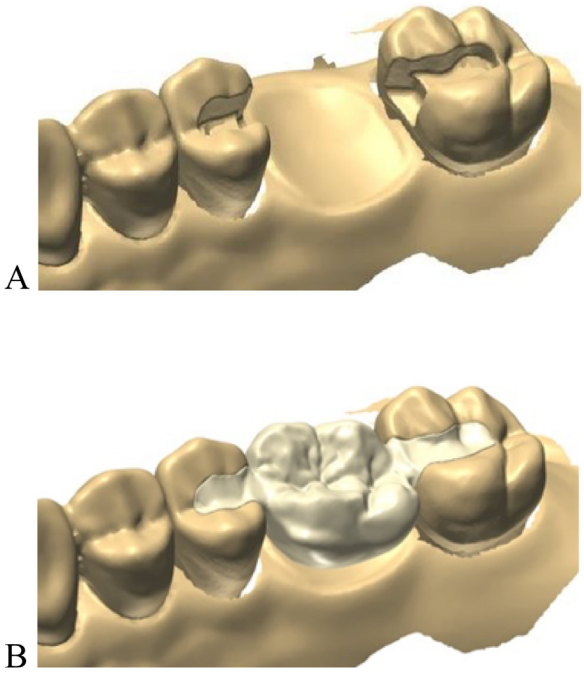

Fig. 1 – 3D view of the used data set. A, preparation. B, with a monolithic IRFPD designed by use of dental design software.

2. Material and methods

2.1. *In-vitro test set-up*

The FEA model was based on an in-vitro test setup (Fig. 1) used to determine the fracture resistance of veneered and monolithic zirconia-based IRFPDs [21]. In that test, IRFPDs were fabricated with anatomic congruence of the FPD-abutment complex, i.e., both monolithic and veneered IRFPDs had the same external geometry. This was achieved by first designing the monolithic IRFPD and then splitting the monolithic design into an anatomically reduced framework and a veneer structure (Fig. 2). The IRFPDs were adhesively bonded to cobalt–chromium abutment teeth. The occlusal boxes of the inlay retainers had a depth of 1.5 mm and a width of 2 mm at the premolar and 3 mm at the molar; the proximal boxes were 2 mm deeper than the occlusal boxes, with an axial reduction of 1.5 mm and a width of 3 mm. The abutment teeth were fabricated with standardized roots (length: 10 mm; cervical/apical cross-sectional areas: $6 \times 10\ mm^2/3 \times 5\ mm^2$), which were covered with heat-shrink tubing to simulate periodontal mobility (Protect; Bahag AG). The apical end of the shrink tubing reached 2 mm beyond the abutment tooth and was sealed with low-viscosity polyvinyl siloxane impression material (Flexitime Correct Flow; Heraeus Kulzer GmbH). The

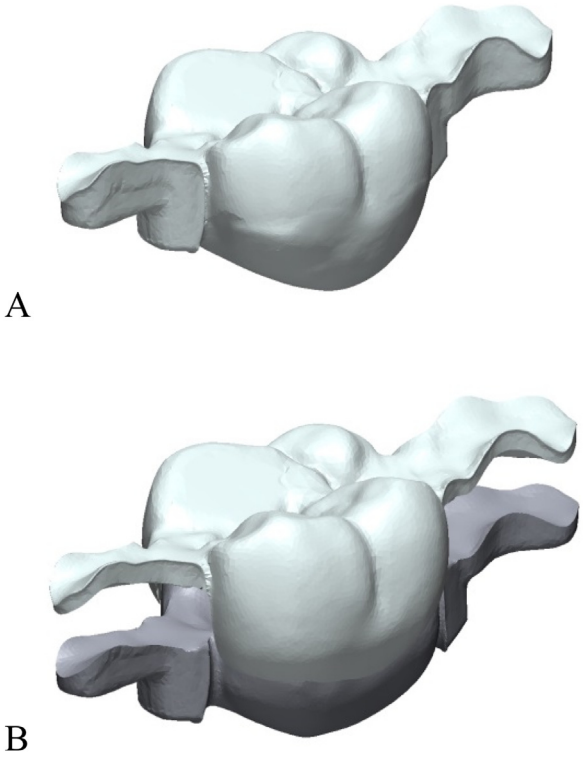

Fig. 2 – IRFPDs with modified mesiopalatal cusp for standardized load application. A, monolithic IRFPD. B, monolithic IRFPD separated into veneer and framework.

Fig. 3 – In-vitro test model with adhesively cemented IRFPD.

abutment teeth with artificial periodontium were then embedded in aluminum blocks by use of autopolymerizing resin (Technovit 4071; Heraeus Kulzer GmbH; Fig. 3). In this arrangement, the abutment teeth had an in-vitro resilience of 0.1 mm per 100 N with respect to vertical loading and about twice that value for horizontal loads. In the in-vitro test, load was applied to the mesiopalatal cusp of the pontic with standardized loading sites (tilted by 60° relative to the direction of insertion).

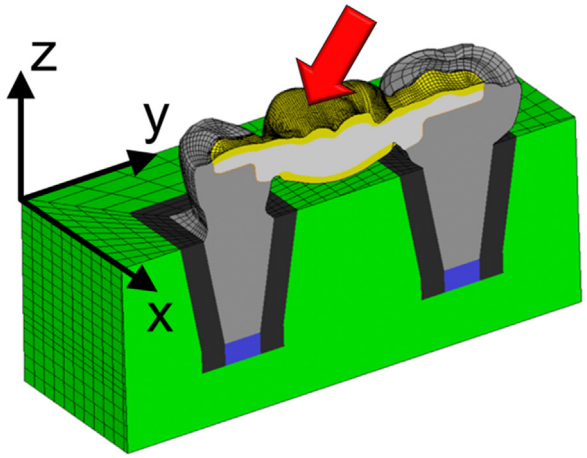

Fig. 4 – Finite element model of veneered (yellow) IRFPD (red arrow shows the oblique loading condition) and coordinate system used (x-direction: buccal-oral; y-direction; mesio-distal; z-direction: vertical).

Table 1 – Properties of materials used in the finite element analysis (FEA) (*determined by FEA achieving the same tooth resilience as calculated in the in-vitro tests).

		Elastic modulus [GPa]	Poisson's ratio [–]
Ceramics	Zirconia	210 [28]	0.26
	Veneering ceramic	70 [28]	0.20
Cement		2–20 [27]	0.35
Tooth material	Unfilled resin	3 [27]	0.35
	Composite resin	10 [37]	0.35
	Dentin	18 [29]	0.30
	Titanium	110 [30]	0.30
	Cobalt–chromium	200 [29]	0.30
Simulated periodontium	Heat-shrink tubing	0.014*	0.35
	Silicone	0.001	0.40
Acrylic resin		2.5 [29]	0.35

2.2. *Finite element analysis*

2.2.1. *Pre-processing*

The stl-data files (preparation scans of the abutment teeth and computer-aided designed (CAD) surface of the modeled restoration with veneer) were reverse engineered by sectioning the surfaces (Geomagic DesignX; 3D Systems) and using these cross-sections to generate a CAD volume model (ANSYS 18.2; CADFEM). The CAD model was then meshed predominantly with hexahedral elements (approx. 230,000 elements; Fig. 4). Accuracy of $7 \pm 20\,\mu m$, root mean square: $21\,\mu m$, was achieved when comparing the meshed FE model and the original dental design stl-data files.

Homogenous, isotropic, and linear-elastic behavior (cf. Table 1) was assumed for all materials. A perfect bond at the luted interfaces was also assumed.

Since the monolithic IRFPD had the same external geometry as the veneered IRFDP, it could be simulated by setting the material properties of the veneer section to those of zirconia.

Calculations were performed for cements with different elastic moduli (2–20 GPa). Cements with elastic moduli of

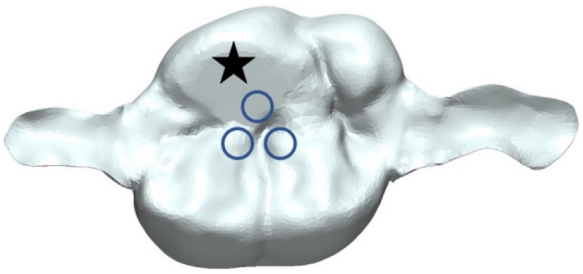

Fig. 5 – IRFPD with marked contact points for oblique loading (star) and for axial loading (blue circles).

2–8 GPa correspond to adhesive cements whereas classical definitive cements, for example zinc phosphate cement or glass ionomer cement, have elastic moduli in the range 10–20 GPa. The fit of the inlays was set to exactly 20 μm at the margin and to 60 μm for the internal cement gap.

The effect of different tooth materials was evaluated in the FEA. Calculations were performed for abutment teeth made from unfilled resin, composite resin, dentin, titanium, and cobalt–chromium alloy.

In addition, computations were carried out both with and without a resilient embedding (heat-shrink tubing, silicone) to investigate the effect of varying abutment tooth resilience. For abutment teeth without additional resilience, material properties of the acrylic resin were overtaken for the volume sections of heat-shrink tubing and silicone.

A constant load of 1000 N was applied to the pontic and two types of load were simulated by varying the loading direction: oblique loading and axial loading. For oblique loading, the load was applied via one contact point on the mesiobuccal cusp of the pontic. The load vector was perpendicular to the cusp surface, which was tilted by 60° with respect to the tooth axis. For axial loading, the vertical force was split into 3 force vectors applied at the contact points of a sphere with 6 mm in diameter placed in the central fossa. Each of the 3 split vectors was oriented perpendicular to the surface (Fig. 5). As a simplification, each load vector was directly applied to surface nodes instead of performing a contact analysis. Since no fractures originated from the loading site in the in-vitro tests, this simplification was justified since for equivalent load cases stresses within the restoration will not differ at some distance from the loading site (Saint-Venant's principle), in particular stresses within the connectors and inlay retainers. Stresses in the vicinity of the loading site were later-on not included in the evaluation. Displacement of nodes at the circumferential and bottom surfaces of the resin block was restricted in all directions. The residual thermal stresses within the ceramic (zirconia: $\alpha_T = 10.5\,10^{-6}K^{-1}$, veneer: $\alpha_T = 10.0\,10^{-6}K^{-1}$ [28]) resulting from the firing process were calculated in advance.

2.2.2. *Post-processing*

The effects of tooth material, tooth resilience, IRFPD design, loading direction, and stiffness of the cement layer were evaluated by use of finite element analysis software (ANSYS 18.2). For brittle materials such as ceramics, it was assumed that critical tensile stresses within the restoration would cause failure. Therefore, estimation of ultimate fracture loads (F_u) was based on the hypothesis of maximum principal stress, i.e., the fracture occurs when the maximum first principal stress, $\sigma_{1,max}$, exceeds the tensile strength, σ_u, of the material. For ceramic materials, properties such as strength vary substantially, i.e., strength values σ_u depend on the failure probability P (Table 2). Accordingly, fracture resistance $F_u(P)$ for P = 10, 50, and 90% failure probability was calculated by use of the equation:

$$F_u(P) = \frac{\sigma_u(P) \cdot 1000N}{\sigma_{1,max}(F = 1000N)}$$

Table 2 – Tensile strengths [MPa] for failure probabilities of 10, 50, and 90% for zirconia (provided by the manufacturer) and veneering ceramics [28].

Failure probability (%)	Zirconia (Cercon hat, Dentsply Sirona)	Veneering ceramics (Cercon Ceram Press, Dentsply Sirona)
10	931	95
50	1155	108
90	1379	120

For veneered restorations, a load corresponding to crack formation in the veneer (initial damage) was evaluated in addition to the failure load of the complete restoration.

Relative fracture loads were calculated to evaluate the effect of tooth mobility and material for the clinically assumed case, i.e., natural abutment teeth with periodontal resilience and adhesively inserted IRFPDs. Here, cement with an elastic modulus of 6 GPa was chosen, corresponding to an adhesive resin cement (Panavia 21; Kuraray Europe GmbH).

In addition to stresses, the relative movement of the abutment teeth in the loaded state was of interest. For quantitative analysis, best fitting rigid body movements transferring the respective nodes of the horizontal cross sections through each abutment tooth at the coronal end of the conical root (identical to the top level of the resin block) from their unloaded position to their position under load were calculated for different combinations of variables.

3. Results

All variables in the FEA affected the calculated fracture resistance of the restorations.

Lateral deflection in the y-direction and tilting around the x-axis of abutment teeth was much greater in restorations with resiliently supported abutment teeth than in the corresponding models without simulated tooth resilience. The example in Fig. 6 shows relative movement of 20 μm in the most coronal part of the root section and 62 μm in the area of the root tip when tooth resilience was included. For restorations without resiliently supported teeth, in contrast, the abutment teeth were deflected only 1.7 μm in the most coronal part of the root section and 2.9 μm at the root tip.

Because of the high longitudinal stiffness of the IRFPD, relative movement in the y-direction (Fig. 7, left) is approximately 0 μm at the inlay level. Thus, the tilt relative to the x-axis did correlate with changes in distance at the most coronal part of the root section. Another, independent, mode of relative movement was caused by rotations of the abutment

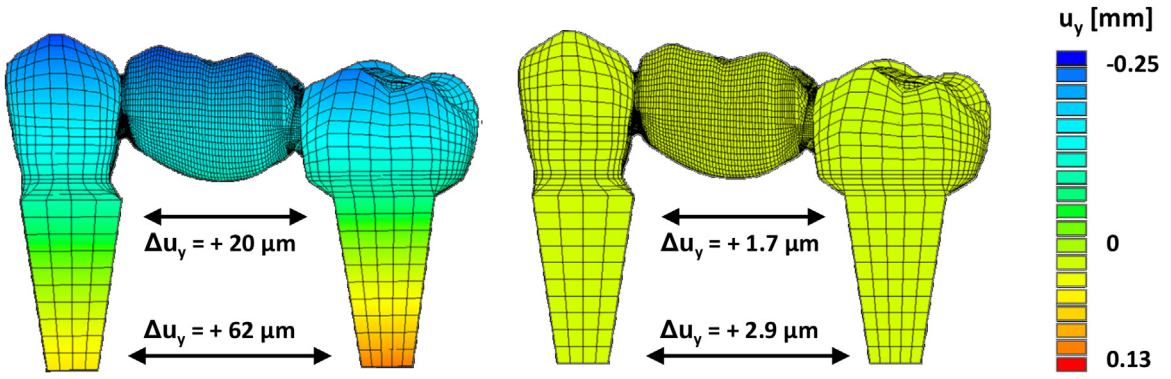

Fig. 6 – Changes in distance in the y-direction at the cervix and root tip between abutment teeth made from CoCr alloy for a monolithic IRFPD and an oblique loading force of 1000 N (color plot: displacements u_y including rigid body movement). Left, with additional abutment tooth resilience. Right, without additional abutment tooth resilience.

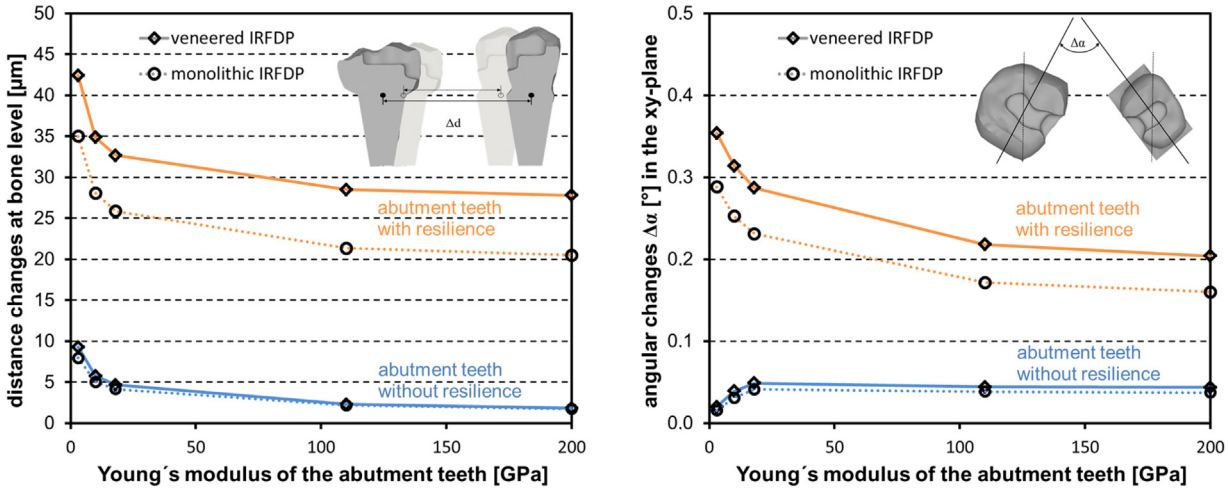

Fig. 7 – Relative distance (left) and angular (right) changes between abutment teeth for oblique loading force of 1000 N measured at the most coronal part of the root sections (identical to bone level) depending on Young's modulus of the abutment teeth and IRFPD design. Cement stiffness had a minor effect, results in this diagram are given for E_{cem} = 6 GPa.

teeth around their respective tooth axes which are parallel to the z-axis (Fig. 7, right). Only the variables abutment tooth material and tooth resilience strongly affected the relative movement of the abutment teeth. Lack of tooth resilience in particular resulted in a drastic reduction in relative movement and, therefore, in much less bending deformation within the IRFPD.

For the adhesively cemented monolithic IRFPD under oblique loading on resiliently supported abutment teeth, the FEA revealed stress concentration zones of different intensities and distributions depending on the tooth material. First principal stresses at the junctions of occlusal and proximal box of the inlays increased tremendously with decreasing abutment tooth stiffness. For the examples shown in Fig. 8, maximum tensile stresses in the inlay regions amounted to 1442 MPa (resin abutment teeth), 707 MPa (natural abutment teeth), and 248 MPa (CoCr abutment teeth). In the also highly stressed connector regions, however, first principal stresses increased slightly with increasing abutment tooth stiffness. For the shown examples, maximum tensile stresses in the basal parts of the connectors were found to be 761 MPa (resin abutment teeth), 806 MPa (natural abutment teeth), and 870 MPa (CoCr abutment teeth). Overall, maximum principal stresses were found in the inlay regions for abutment teeth with low stiffness (resin: 1442 MPa) and in the connector region for abutment teeth with moderate and high stiffness (dentin: 806 MPa, CoCr: 870 MPa).

With regard to the effect of abutment tooth mobility and material on relative fracture strength for 50% failure probability for zirconia, it was found that the effect of the Youngs modulus of the cement was very small. When using abutment teeth made from dentin, unfilled resin, or composite resin, fracture resistance increased slightly as the Youngs modulus of the cement increased.

When unfilled resin teeth were used, fracture resistance was underestimated by 50–57%, regardless of the abutment tooth bedding.

Fracture resistance was also underestimated if the restorations were cemented on resiliently supported composite resin abutment teeth (11–23%).

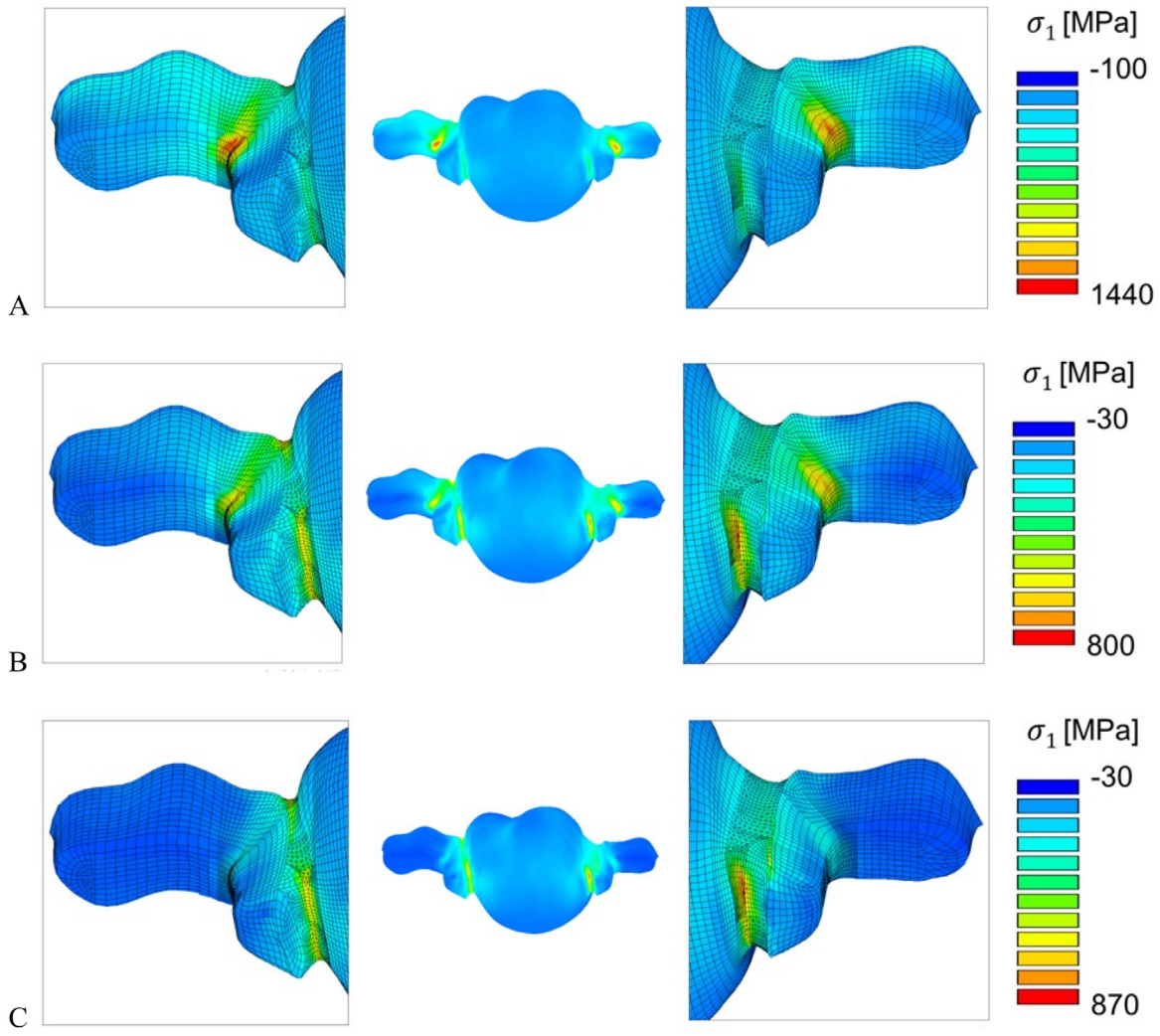

Fig. 8 – First principal stresses for monolithic IRFPDs cemented on teeth, A, made from unfilled resin. B, made from dentine. C, made from cobalt–chromium.

For metal abutment teeth (CoCr), tooth resilience greatly affected the fracture force. When tooth resilience was simulated, fracture forces deviated only slightly from the reference (from −6% to +15%) whereas a rigid support (without periodontal resilience) was likely to lead to overestimation of fracture resistance by a factor of 1.50–1.95. Almost the same results could be observed for titanium abutment teeth (from −6% to +17%).

The effect of abutment tooth material on crack formation within the veneering ceramics (failure load of the veneering ceramics) was small when resiliently supported abutment teeth were used (Table 3). Here, in critical regions with respect to mechanical loading, thermal prestresses ranged from about −20 MPa to −40 MPa and had, therefore, a positive effect on the load bearing capacity.

Comparison of the 50% failure probability for monolithic and veneered IRFPDs with axial and oblique loading revealed no difference between the two loading conditions when the abutment teeth were resiliently supported. For rigidly supported abutment teeth, overestimation of the fracture load was observed for the zirconia and the veneering ceramic. Overestimation increased the greater the elastic modulus of the abutment teeth: by up to 130% for zirconia, and by up to 300% for the veneering ceramic (Fig. 10).

Table 3 – Calculated relative fracture loads [%] of the veneer for oblique loading at a failure probability of P = 50%, summarized for the investigated range of Youngs moduli of the cement.

	Abutment teeth with resilience	Abutment teeth without resilience
CoCr	95–99	134–135
Titanium	96–100	136–138
Dentin	99–101	131–132
Composite resin	99–100	128–129
Unfilled resin	93–94	98–103

Comparison of fracture loads from the previous in-vitro test [20] with those calculated in the FEA revealed good agreement between values in the event of a failure of the zirconia material (Fig. 11).

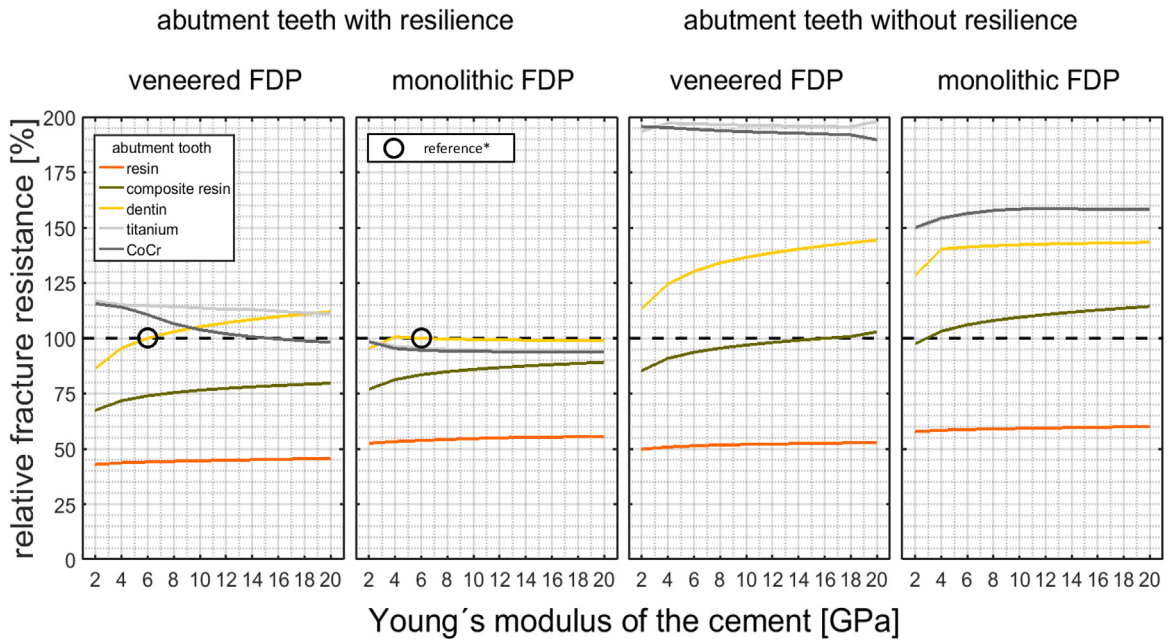

Fig. 9 – Relative fracture resistance at 50% failure probability calculated for zirconia.
***Dentine, resiliently supported abutment teeth, adhesive cementation (Panavia).**

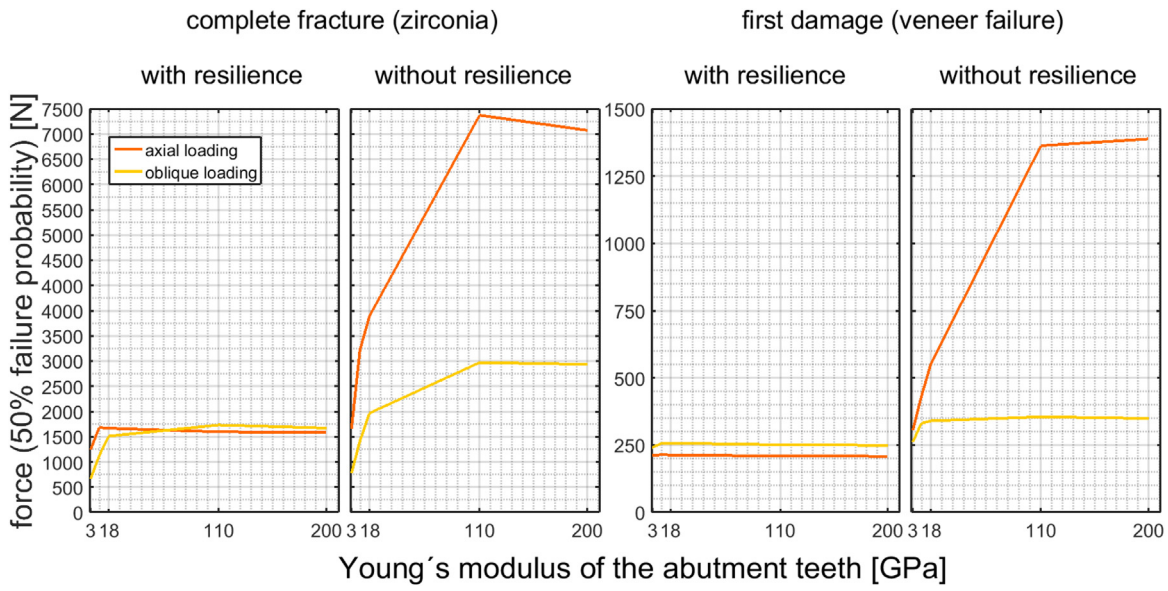

Fig. 10 – Comparison of axial and oblique loading for zirconia and veneering ceramic for 50% failure probability.

Detection of failures within the veneering ceramic (initial damage) by use of FE analysis resulted in lower fracture loads than those found in in-vitro tests. Here initial damage (failure of the veneer) was correlated to test forces at which a macroscopic visible crack could be identified.

4. Discussion

For successful FEA, exact transfer of geometry and use of realistic material properties and boundary conditions are essential. To ensure the best possible applicability of FE results to the clinical situation, therefore, the best match possible should be achieved between the dental design data file and the finite element surface. In this study, deviation of the FE surfaces from the dental design data file was $7 \pm 20\,\mu m$, RMS: $21\,\mu m$. Deviations were mainly caused by very slight changes in the connector area. For reasons of geometric simplification and optimal mesh quality, the boundaries of the veneering ceramic volume were slightly modified. Furthermore, the CAD surface from the dental construction process had small flaws which had to be removed during reverse engineering (these flaws are neglected by the milling process, but would affect

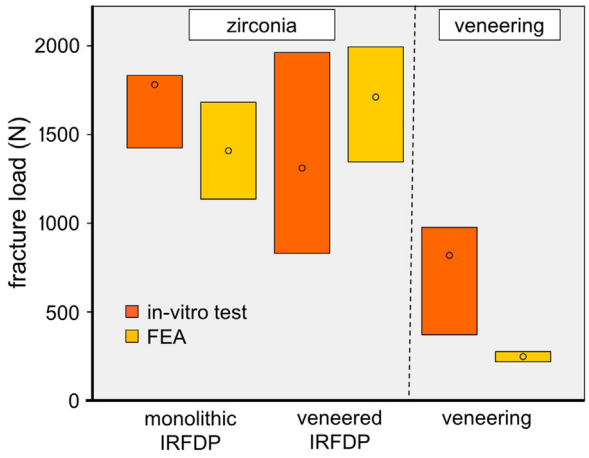

Fig. 11 – Comparison of failure loads determined in vitro and those derived from finite element analysis. Upper bar edge: P = 90%, circle: P = 50%, lower bar edge: P = 10%.

the FEA). The veneering ceramic ended at the mesial or distal preparation margin of the inlay. The basal connector area was constructed without ceramic veneer, similar to the veneering design attempted manually in dental production [21], because it has been shown that, with regard to the load-bearing capacity of bilayered ceramic systems, it seems reasonable to avoid veneering, particularly in those areas where tensile stresses occur [26].

In this study, linear elastic and isotropic behavior was assumed for all materials. This is in agreement with former FEA investigations [27–30], but is also a limitation of this study. Whereas the behavior of ceramic materials is isotropic and almost perfectly linear elastic until fracture, that of hard natural tissues (bone, dentin, enamel) is, in general, anisotropic and linear elastic whereas soft natural tissues (periodontal ligament) show anisotropic and non-linear viscoelastic behavior. Since the exact stresses within the abutment teeth and elements used for fixation were not of interest but a realistic simulation of their resilience when supporting the IRFPD, these simplifications are reasonable. Small geometric imperfections, which are inevitable in dental manufacturing, were not taken into consideration. Variations in material strength, e.g. caused by induced damage during the manufacturing process, were taken into account by transferring the scatter found in the standardized strength test to this analysis.

When abutment teeth made from dentin were used, the enamel and pulp were not modeled. Because the literature indicates that the pulp has a negligible or no effect on stress distribution in dental restorations, this seemed acceptable [31]. These statements were, however, made in relation to veneers, i.e. the biomechanical behavior of teeth prepared for inlays could, in contrast, be affected. Enamel, which has a substantially higher modulus of elasticity than dentin, is absent in the mathematical model; this results in a more rigorous test setup because of increased resilience of the natural abutment tooth [29].

Comparison of fracture loads calculated from maximum tensile stresses derived from the FEA with those found in the in-vitro tests showed that the theoretical fracture loads corresponded to experiments quite well for total fractures (fracture within zirconia). For initial crack formation within the veneering ceramic (initial damage), FEA results were more conservative than those found in the experiments: FEA indicated critical forces of 250–300 N, significantly below the threshold of 500 N used for approval of clinical use in the posterior region [1–3], compared with the critical forces of 400–900 N (Fig. 9) observed in the experiments. In the in-vitro test, however, initial damage was associated with the formation of a larger, usually macroscopically visible, crack. With regard to the FEA findings, it can be assumed that either the initial cracking started before the time at which the crack became visible or a hairline crack in the most critical region near the boundary of the veneer at the basal surfaces of the connectors did not propagate any further and another crack in less stresses regions (which was initiated at higher loads) grew to a visible size. Clinically, that would indicate that initial crack formation within the veneering ceramics might have begun at force magnitudes below 500 N. This explains the results of several in-vivo studies in which chipping was the first major type of failure and occurred at an early stage [16,32].

Considering the effect of tooth mobility and abutment tooth material, the cement had only a small effect and could be discounted.

Previous studies have shown that all-ceramic FDPs cemented on metal abutment teeth had a 30% higher fracture load than those on resin abutment teeth [22,33]. In these studies, full crowns were used as retainers. But these results cannot be applied to IRFPDs. In the case of full crowns, the loaded restoration is supported by the abutment teeth, resulting in higher fracture loads. The higher the Young's modulus of the abutment teeth, the greater is this effect. As reported in the results section, a similar strong correlation could only be seen when looking solely at the inlay retainers. In contrast, bending of the IRFPD was the more "concentrated" to the connector regions the stiffer the abutment teeth, which caused stresses there to increase (slightly) with increasing abutment tooth stiffness. This led to a change in the overall critical region when varying the abutment tooth stiffness (cf. Fig. 8): Whereas, based on the FEA and failure probabilities given by the distribution of material strength, fractures trough the inlay retainers were most probable at rather low test forces, fracture through the connector(s) was the predominant failure mode when using abutment teeth with moderate or high stiffness and be associated with a higher fracture resistance. This explains the good correlation of fracture load associated with natural and metal abutment teeth.

Furthermore, it showed that the expected fracture patterns can differ when different abutment tooth materials are used. If the fracture patterns of the in-vitro test [21] (fracture through the connector area was the predominant failure mode) are compared with the areas with the highest tensile stress detected by the FEA using metal abutment teeth, good conformity could be seen. If non-natural teeth are to be used for in-vitro experiments on IRFPDs, it can be concluded that, concerning the fracture pattern, metal teeth are superior to resin ones.

On the basis of these findings, it is not surprising that use of abutment teeth made from unfilled resin will lead to underestimation of the fracture load (up to 57%) applied to zir-

conia, irrespective of restoration design and support type. As expected, relative fracture resistance of metal abutment teeth (titanium and CoCr) was close to the clinically assumed case (titanium: from −6% to +17%; CoCr: from −6% to +15%) when tooth resilience was simulated. In contrast, a rigid support (without periodontal resilience) is likely to lead to overestimation of fracture resistance by a factor of 1.50–1.95.

With regard to the veneering ceramic, the effect of abutment tooth material on crack formation within the veneering ceramic (failure load of the veneering ceramic) is only small when resiliently supported abutment teeth are used. For rigidly supported metal abutment teeth, overestimation (up to 35%) of loads is seen, corresponding to veneer failure.

According to the findings of this FEA, the use of resiliently supported metal abutment teeth is recommended when testing all-ceramic IRFPDs in vitro. Wimmer et al. were able to show that the fracture loads of three-unit zirconia fixed dental prostheses (FDPs) cemented on metal abutment teeth were up to 30% higher than those of unfilled resin abutment teeth [22]. Rosentritt et al. also came to this conclusion in their study on the effect of several variables on the fracture loads of all-ceramic FPDs made from Empress 2 [33]. The results from both studies were obtained by use of prostheses anchored by full crowns. For full crowns, the loaded restoration is supported by the abutment teeth. This results in higher fracture loads. The greater the modulus of elasticity of the abutment tooth material, the greater this effect is, as proved by the studies cited above. In a FEA study by Mollers et al., lower tensile stresses were observed for all-ceramic FDPs anchored by full crowns than for all-ceramic IRFPDs under the same load [25,34]. This finding strongly indicated that FEA results for one type of restoration should not be generalized for all types of denture.

Comparisons with other FEAs are difficult because of different underlying material properties, restoration design, loading condition, and finite element model. Some similarities can, however, be observed. Thompson et al. investigated IRFPDs cemented on natural teeth. Restorations were loaded centrally with a force of 200 N. Extrapolation of maximum tensile stresses according to the loads used in this FEA resulted in maximum tensile stresses of 990 MPa [35]. This is comparable to the 800-MPa maximum tensile stresses calculated here. These stresses were also found at the basal surface of the connector. The location of maximum tensile stresses and thus a fracture through the connector is in agreement with other studies [12,21,36].

Because of these above-mentioned restrictions and necessary simplifications and selection of distinct situations, promising FE results still have to be confirmed by controlled clinical trials before a final recommendation can be made.

5. Conclusion

In the FE analysis, loads were affected by all test variables, corresponding to veneer failure or total failure of zirconia-based IRFPDs. To obtain valid in-vitro results with clinical applicability, zirconia-based IRFPDs should be tested on resiliently supported metal abutment teeth.

First principal stresses at the inlay retainers and the connectors were affected differently by changes in stiffness of the supporting structures. This finding clarifies that it cannot be recommended to generalize findings of FE analyses for FDPs with completely different geometry and boundary conditions.

REFERENCES

[1] Ferrario VF, Sforza C, Serrao G, Dellavia C, Tartaglia GM. Single tooth bite forces in healthy young adults. J Oral Rehabil 2004;31:18–22.

[2] Regalo SC, Santos CM, Vitti M, Regalo CA, de Vasconcelos PB, Mestriner Jr W, et al. Evaluation of molar and incisor bite force in indigenous compared with white population in Brazil. Arch Oral Biol 2008;53:282–6.

[3] Fontijn-Tekamp FA, Slagter AP, Van Der Bilt A, Van 'T Hof MA, Witter DJ, Kalk W, et al. Biting and chewing in overdentures, full dentures, and natural dentitions. J Dent Res 2000;79:1519–24.

[4] Tinschert J, Natt G, Mautsch W, Augthun M, Spiekermann H. Fracture resistance of lithium disilicate-, alumina-, and zirconia-based three-unit fixed partial dentures: a laboratory study. Int J Prosthodont 2001;14:231–8.

[5] Studart AR, Filser F, Kocher P, Gauckler LJ. Fatigue of zirconia under cyclic loading in water and its implications for the design of dental bridges. Dent Mater 2007;23:106–14.

[6] Sax C, Hammerle CH, Sailer I. 10-year clinical outcomes of fixed dental prostheses with zirconia frameworks. Int J Comput Dent 2011;14:183–202.

[7] Raigrodski AJ, Hillstead MB, Meng GK, Chung KH. Survival and complications of zirconia-based fixed dental prostheses: a systematic review. J Prosthet Dent 2012;107:170–7.

[8] Sailer I, Gottnerb J, Kanelb S, Hammerle CH. Randomized controlled clinical trial of zirconia-ceramic and metal-ceramic posterior fixed dental prostheses: a 3-year follow-up. Int J Prosthodont 2009;22:553–60.

[9] Schmitt J, Goellner M, Lohbauer U, Wichmann M, Reich S. Zirconia posterior fixed partial dentures: 5-year clinical results of a prospective clinical trial. Int J Prosthodont 2012;25:585–9.

[10] Raigrodski AJ, Chiche GJ, Potiket N, Hochstedler JL, Mohamed SE, Billiot S, et al. The efficacy of posterior three-unit zirconium-oxide-based ceramic fixed partial dental prostheses: a prospective clinical pilot study. J Prosthet Dent 2006;96:237–44.

[11] Rinke S, Gersdorff N, Lange K, Roediger M. Prospective evaluation of zirconia posterior fixed partial dentures: 7-year clinical results. Int J Prosthodont 2013;26:164–71.

[12] Wolfart S, Ludwig K, Uphaus A, Kern M. Fracture strength of all-ceramic posterior inlay-retained fixed partial dentures. Dent Mater 2007;23:1513–20.

[13] Puschmann D, Wolfart S, Ludwig K, Kern M. Load-bearing capacity of all-ceramic posterior inlay-retained fixed dental prostheses. Eur J Oral Sci 2009;117:312–8.

[14] Kilicarslan MA, Kedici PS, Kucukesmen HC, Uludag BC. In vitro fracture resistance of posterior metal-ceramic and all-ceramic inlay-retained resin-bonded fixed partial dentures. J Prosthet Dent 2004;92:365–70.

[15] Ohlmann B, Gabbert O, Schmitter M, Gilde H, Rammelsberg P. Fracture resistance of the veneering on inlay-retained zirconia ceramic fixed partial dentures. Acta Odontol Scand 2005;63:335–42.

[16] Rathmann F, Bomicke W, Rammelsberg P, Ohlmann B. Veneered zirconia inlay-retained fixed dental prostheses: 10-year results from a prospective clinical study. J Dent 2017;64:68–72.

[17] Aboushelib MN, Feilzer AJ, Kleverlaan CJ. Bridging the gap between clinical failure and laboratory fracture strength

tests using a fractographic approach. Dent Mater 2009;25:383–91.
[18] Rues S, Kroger E, Muller D, Schmitter M. Effect of firing protocols on cohesive failure of all-ceramic crowns. J Dent 2010;38:987–94.
[19] Ereifej N, Silikas N, Watts DC. Initial versus final fracture of metal-free crowns, analyzed via acoustic emission. Dent Mater 2008;24:1289–95.
[20] Bomicke W, Rues S, Hlavacek V, Rammelsberg P, Schmitter M. Fracture behavior of minimally invasive, posterior, and fixed dental prostheses manufactured from monolithic zirconia. J Esthet Restor Dent 2016;28:367–81.
[21] Bomicke W, Waldecker M, Krisam J, Rammelsberg P, Rues S. In vitro comparison of the load-bearing capacity of ceramic and metal-ceramic resin-bonded fixed dental prostheses in the posterior region. J Prosthet Dent 2018;119:89–96.
[22] Wimmer T, Erdelt KJ, Eichberger M, Roos M, Edelhoff D, Stawarczyk B. Influence of abutment model materials on the fracture loads of three-unit fixed dental prostheses. Dent Mater J 2014;33:717–24.
[23] Rosentritt M, Behr M, Scharnagl P, Handel G, Kolbeck C. Influence of resilient support of abutment teeth on fracture resistance of all-ceramic fixed partial dentures: an in vitro study. Int J Prosthodont 2011;24:465–8.
[24] Alkharrat AR, Schmitter M, Rues S, Rammelsberg P. Fracture behavior of all-ceramic, implant-supported, and tooth-implant-supported fixed dental prostheses. Clin Oral Invest 2017;22:1663–73.
[25] Mollers K, Patzold W, Parkot D, Kirsten A, Guth JF, Edelhoff D, et al. Influence of connector design and material composition and veneering on the stress distribution of all-ceramic fixed dental prostheses: a finite element study. Dent Mater 2011;27:e171–5.
[26] Guazzato M, Proos K, Sara G, Swain MV. Strength, reliability, and mode of fracture of bilayered porcelain/core ceramics. Int J Prosthodont 2004;17:142–9.
[27] Wimmer T, Erdelt KJ, Raith S, Schneider JM, Stawarczyk B, Beuer F. Effects of differing thickness and mechanical properties of cement on the stress levels and distributions in a three-unit zirconia fixed prosthesis by FEA. J Prosthodont 2014;23:358–66.
[28] Schmitter M, Lotze G, Bomicke W, Rues S. Influence of surface treatment on the in-vitro fracture resistance of zirconia-based all-ceramic anterior crowns. Dent Mater 2015;31:1552–60.
[29] Schmitter M, Rammelsberg P, Lenz J, Scheuber S, Schweizerhof K, Rues S. Teeth restored using fiber-reinforced posts: in vitro fracture tests and finite element analysis. Acta Biomater 2010;6:3747–54.
[30] Moraes SLD, Verri FR, Santiago JFJ, Almeida DAF, Lemos CAA, Gomes JML, et al. Three-dimensional finite element analysis of varying diameter and connection type in implants with high crown-implant ratio. Braz Dent J 2018;29:36–42.
[31] Chander NG, Padmanabhan TV. Finite element stress analysis of diastema closure with ceramic laminate veneers. J Prosthodont 2009;18:577–81.
[32] Ohlmann B, Rammelsberg P, Schmitter M, Schwarz S, Gabbert O. All-ceramic inlay-retained fixed partial dentures: preliminary results from a clinical study. J Dent 2008;36:692–6.
[33] Rosentritt M, Behr M, Gebhard R, Handel G. Influence of stress simulation parameters on the fracture strength of all-ceramic fixed-partial dentures. Dent Mater 2006;22:176–82.
[34] Mollers K, Parkot D, Kirsten A, Guth JF, Edelhoff D, Fischer H. Influence of tooth mobility on critical stresses in all-ceramic inlay-retained fixed dental prostheses: a finite element study. Dent Mater 2012;28:146–51.
[35] Thompson MC, Field CJ, Swain MV. The all-ceramic, inlay supported fixed partial denture. Part 2. Fixed partial denture design: a finite element analysis. Aust Dent J 2011;56:302–11.
[36] Zhang Z, Thompson M, Field C, Li W, Li Q, Swain MV. Fracture behavior of inlay and onlay fixed partial dentures — an in-vitro experimental and XFEM modeling study. J Mech Behav Biomed Mater 2016;59:279–90.
[37] Ausiello P, Ciaramella S, Martorelli M, Lanzotti A, Gloria A, Watts DC. CAD-FE modeling and analysis of class II restorations incorporating resin-composite, glass ionomer and glass ceramic materials. Dent Mater 2017;33:1456–65.